Analytica Chimica Acta 769 (2013) 40–48

Contents lists available at SciVerse ScienceDirect

Analytica Chimica Acta

journal homepage: www.elsevier.com/locate/aca

Graphene oxide as a nanocarrier for loading and delivery of medicinal drugs and as a biosensor for detection of serum albumin

Yongnian Ni[a,b,*], Fangyuan Zhang[a], Serge Kokot[c]

[a] State Key Laboratory of Food Science and Technology, Nanchang University, Nanchang 330047, China
[b] Department of Chemistry, Nanchang University, Nanchang 330031, China
[c] School of Chemistry, Physics and Mechanical Engineering, Science and Engineering Faculty, Queensland University of Technology, Brisbane 4001, Australia

HIGHLIGHTS

- Studied the loading interaction of HCPT (10-hydroxy camptothecin) on graphene oxide.
- The nature of the interaction between graphene oxide, HCPT and BSA was investigated.
- Studied the HCPT–GO–BSA system with three-way fluorescence spectroscopy and chemometrics.
- A novel BSA biosensor was constructed with improved sensitivity and selectivity.

GRAPHICAL ABSTRACT

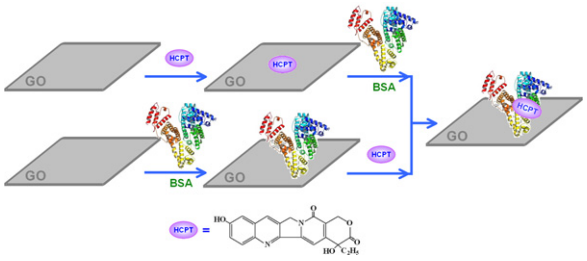

ARTICLE INFO

Article history:
Received 23 November 2012
Received in revised form 10 January 2013
Accepted 16 January 2013
Available online 25 January 2013

Keywords:
Graphene oxide
Nano-carrier
Serum albumin
Fluorescence enhancement
Chemometrics
Biosensor

ABSTRACT

The interaction of graphene oxide (GO), a medicinal drug (10-hydroxy camptothecin (HCPT)), and bovine serum albumin (BSA) was investigated with the aim of developing a method for the analysis of serum albumin proteins. It was demonstrated that HCPT could be readily loaded onto GO via the π–π stacking interaction, and the delivery of HCPT to BSA was improved in the presence of GO; this, in turn, facilitated the binding interaction of HCPT and BSA. Chemometrics methods, multivariate curve resolution-alternating least squares (MCR-ALS) and parallel factor analysis (PARAFAC), were applied to resolve spectral data, and this assisted in the elucidation of the above interaction. GO was found to enhance the fluorescence response of HCPT to BSA, and thus, a low cost fluorescence bio-sensing platform was developed for fluorescence-enhanced detection of BSA based on GO. The satisfactory analytical performance of this biosensor for BSA was attributed to the structure and electronic properties of GO.

1. Introduction

In general, nanomaterial-based drug carriers are of significant research interest at the interface of nanotechnology and biomedicine because they facilitate the efficient loading, targeted delivery and controlled release of medicinal drugs; therefore, they should be useful for biomedical applications [1–6]. Graphene is a single-atom-thick, two-dimensional carbon material that has attracted attention because of its remarkable electronic, mechanical, and thermal properties [7–11]. Potential applications of graphene for nano-electronics [12,13], sensors [14], and nanocomposites [15] have been actively pursued [16], and research on its potential for biological applications has also been reported, e.g. drug loading and delivery. Dai and his colleagues, for the first time, employed polyethylene nano-scale graphene oxide (NGO) as a nano-carrier to load anticancer drugs via non-covalent physisorption [17,18]. Chen and his group found that the doxorubicin hydrochloride, an anticancer drug, loaded on the graphene oxide (GO) with a loading weight ratio of the loaded drug to

* Corresponding author at: Department of Chemistry, Nanchang University, Nanchang 330031, China. Tel.: +86 791 83969500; fax: +86 791 83969500.
E-mail addresses: ynni@ncu.edu.cn (Y. Ni), s.kokot@qut.edu.au (S. Kokot).

0003-2670/$ – see front matter © 2013 Elsevier B.V. All rights reserved.
http://dx.doi.org/10.1016/j.aca.2013.01.038

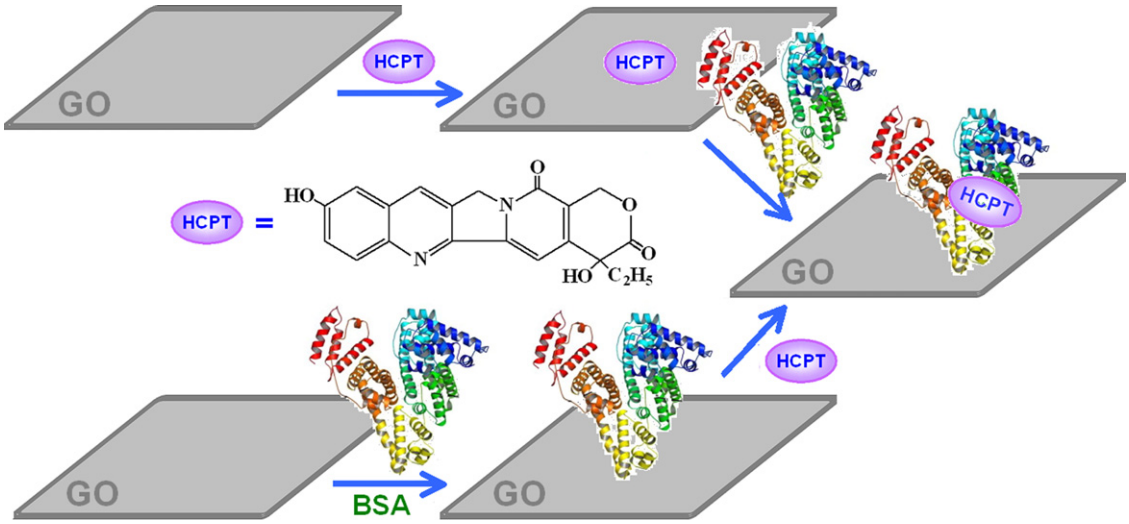

Scheme 1. Schematic representation of the interaction mechanism between HCPT (10-hydroxycamptothecin), BSA, and GO.

carrier as high as 200% [19]. Another group led by Zhang, investigated the controlled loading of two anticancer drugs, doxorubicin and camptothecin, onto the functional NGO via π–π stacking and hydrophobic interactions; they demonstrated that this NGO when loaded with the two drugs, showed specific targeting and remarkably high cytotoxicity to human breast cancer MCF-7 cells, compared to an NGO loaded only with either one of the two drugs [20]. This work demonstrated that GO derivatives can be used as efficient nano-carriers for the loading and delivery of water-insoluble aromatic drugs; this was because GO is comparatively small, has intrinsic optical properties, a large specific surface area, useful non-covalent interactions with aromatic drug molecules, and is relatively cheap. GO has also been used as a platform for the detection of DNA [21,22], proteins [23,24], metal ions [25–27], among other applications [28,29], and all these substances can be analyzed because GO can disperse in water, has a surface that can be readily modified, and can quench photoluminescence.

10-Hydroxycamptothecin (HCPT structure, Scheme 1), a natural camptothecin analog, has shown the strongest anti-tumor effects among its analogs, and clinical evaluations have indicated that HCPT is less toxic than camptothecin itself [30]. However, the clinical use of HCPT has been hampered by its poor water solubility.

Among biomacromolecules, serum albumin (SA) is a soluble protein, which is a major constituent of the circulatory system, and it commonly serves as a depository and a transport molecule for many exogenous compounds [31,32]. Consequently, simple, rapid and low cost analysis for SA proteins would be useful [33,34]. Studies on the binding of drugs with plasma proteins will facilitate the interpretation of the metabolism and transport processes of such substances, and the binding of small molecules with bovine serum albumin (BSA) is a typical example of such interactions. Thus, it is an appropriate protein to use for such investigations, partly because of its structural homology with human serum albumin (HSA) [35].

In general, the interactions of drugs with nanomaterials or biopolymers have been investigated by utilizing UV–vis and fluorescence spectroscopy. Such investigations provided information about the non-covalent binding of drugs on nanomaterials [36], the non-covalent forces and the thermodynamic constants for the binding processes between drugs and biopolymers [37].

Chemometrics methods of data analysis, such as multivariate curve resolution-alternating least squares (MCR-ALS) and parallel factor analysis (PARAFAC), are well known for their ability to resolve spectroscopic data and extract profiles of individual chemical components from composite responses [38]. Such results generate qualitative and quantitative information, which otherwise cannot be obtained by conventional methods, and which consequently, enable further analysis of the problem under investigation as is the case with the biosystems in this work.

The aims of this study were to: 1. investigate the interaction of HCPT/GO/BSA in aqueous solution with the use of UV–vis and fluorescence techniques and other methods as required; 2. research and develop a spectroscopic method for BSA analysis using the HCPT molecule in conjunction with the GO platform as the essential molecular, analytical tool.

2. Experimental

2.1. Materials

GO was synthesized by the modified Hummer's method (Dr. Qiu, Nanchang University, Nanchang, China). Bovine serum albumin (BSA, $M = 66{,}000$) was free of fatty acids and an electrophoresis grade reagent (99% pure; Huamei Biological Co. Ltd., Shanghai, China). HCPT (Huangshi Feiyun Pharmaceutical Co. Ltd., Hubei, China) was used as received. All other reagents were of analytical grade, and doubly distilled water was used throughout. All solutions used in the experiments were adjusted with the Tris–HCl buffer (0.05 mol L^{-1}, pH 7.4).

2.2. Apparatus

UV–vis absorption spectra were recorded with an Agilent 8453 spectrophotometer (Aglient Instruments, USA) using a 1.0 cm quartz cell. The fluorescence spectra, three-way excitation-emission fluorescence spectra, and resonance light scattering spectra were collected with a Perkin Elmer LS-55 luminescence spectrometer (PerkinElmer Instruments, USA) equipped with a thermostatic bath (Model ZC-10, Ningbo Tianheng Instruments Factory, China) and a 1.0 cm quartz cell. The atomic force microscopic (AFM) images were obtained by using an AJ-III instrument (Shanghai Aijian Nanotechnology, China) in the tapping mode, which also produced simultaneously the intensity and phase data. Standard silicon cantilevers (spring constant: 0.6–6.0 N m^{-1}) were used at their resonance frequencies (typically 60–150 kHz). All measurements were carried out at a temperature of 25.0 ± 0.5 °C unless otherwise stated.

2.3. Experimental procedure

2.3.1. Investigation of loading interaction of HCPT on GO

GO was exfoliated by sonication under ambient conditions for 20 min. Loading of HCPT on GO was carried out by mixing HCPT with the GO aqueous suspension – the unbound HCPT was removed by centrifugation. The UV–vis spectra (200–900 nm) of HCPT (0.25 $\mu g\,mL^{-1}$), GO (8.0 $\mu g\,mL^{-1}$), and their mixed solution were obtained. Fluorescence spectra were collected by adding GO (0.0–19.2 $\mu g\,mL^{-1}$ at intervals of 0.8 $\mu g\,mL^{-1}$) to the HCPT solution (0.83 $\mu g\,mL^{-1}$) to investigate any fluorescence quenching of HCPT by GO in the range of 300–650 nm (excitation wavelength: 320 nm).

2.3.2. Fluorescence quenching experiments

Fluorescence spectra of BSA (1.0×10^{-7} mol L^{-1}) in the presence of HCPT (0–4.56×10^{-7} mol L^{-1} at intervals of 0.46×10^{-7} mol L^{-1}) were measured at two constant temperatures (298 and 308 K). Each sample solution was allowed to stand for 5 min, and then scanned in the range of 250–650 nm with an excitation wavelength of 280 nm. Another quenching experiment was conducted in the presence of GO (2.96 $\mu g\,mL^{-1}$) under the same conditions.

The fluorescence quenching of BSA by GO was measured by adding GO (0.0–2.7 $\mu g\,mL^{-1}$ at intervals of 0.34 $\mu g\,mL^{-1}$) to the BSA (1.0×1.0^{-7} mol L^{-1}) solution in the range of 250–650 nm (excitation wavelength: 280 nm).

2.3.3. Three-way excitation-emission fluorescence experiments

Two three-way excitation-emission fluorescence experiments were carried out for two cases – with and without GO (2.0 $\mu g\,mL^{-1}$). Concentration of BSA was kept at 1.67×10^{-7} mol L^{-1}; the added HCPT concentration was in the range of 0.00–7.30×10^{-7} mol L^{-1} at intervals of 4.84×10^{-8} mol L^{-1} (total: 17 solutions). The fluorescence spectra for all these solutions were recorded in the excitation wavelength range of 200–400 nm (every 5 nm, total: 41 points), and the emission wavelength of 250–600 nm range (every 0.5 nm, total: 701 points). Thus, two three-way excitation-emission fluorescence matrices (EEM) were obtained (17 (samples) × 41 (λ_{ex}) × 701 (λ_{em})).

2.3.4. BSA detection

BSA was added to the HCPT–GO solution in the concentration range of 0.00–7.98×10^{-7} mol L^{-1} at intervals of 1.33×10^{-7} mol L^{-1}. The fluorescence spectra were recorded in the range of 300–700 nm at an excitation wavelength of 320 nm. Two types of control experiment were performed: (1) adding BSA to the HCPT solution directly (i.e. without GO), and (2) replacing BSA, in turn, by one of lysozyme, pepsin, and trypsin, respectively, under the same conditions as above.

2.3.5. Resonance light scattering

Resonance light scattering spectra were obtained by simultaneously scanning the excitation and emission monochromators ($\Delta\lambda = 0$ nm) of the spectrofluorometer from 250 to 650 nm with the excitation slit set at 10 nm and the emission slit at 2.5 nm.

2.3.6. Atomic force microscope study

Muscovite mica was cut into about 1.2 cm × 1.2 cm square pieces as substrate. Samples for the AFM imaging were prepared by depositing 10 μL of the sample solutions of GO, HCPT–GO, BSA–GO, and HCPT–BSA–GO on freshly cleaved mica plates, which were dried overnight.

2.4. Principles of fluorescence quenching

Fluorescence quenching is described by the well-known Stern–Volmer equation [39]:

$$\frac{F_0}{F} = 1 + K_q\tau_0 = 1 + K_{SV}[Q] \quad (1)$$

where F_0 and F are the fluorescence intensities before and after addition of the quencher, respectively. K_q is the quenching rate constant of the biomolecule; K_{SV} is the Stern–Volmer quenching constant; [Q] is the concentration of the ligand. K_{SV} was determined from the linear regression plot of (F_0/F) versus [Q].

For static quenching, the relationship between fluorescence quenching intensity and the concentration of quencher follows the equation [40]:

$$\log\left[\frac{F_0/F}{F}\right] = \log K_a + n\log[Q] \quad (2)$$

where K_a and n are the apparent binding constant to a site and the number of binding sites, respectively.

In general, the molecular forces contributing to the interactions of small molecules with proteins include hydrogen bonding, Van der Waals forces, electrostatic forces, and the hydrophobic interactions [41]; the thermodynamic parameters are the enthalpy change (ΔH) and entropy change (ΔS). If ΔH is assumed to be constant over a given temperature range, then the values of ΔH and ΔS can be evaluated using the van't Hoff equation [42]:

$$\ln K = -\frac{\Delta H}{RT} + \frac{\Delta S}{R} \quad (3)$$

where K is analogous to the binding constants, K_a, at the corresponding temperatures (298 and 308 K); R is the gas constant. The free energy change (ΔG) can be calculated from the following equation:

$$\Delta G = \Delta H - T\Delta S = -RT\ln K \quad (4)$$

2.5. Chemometrics methods

Multivariate curve resolution-alternating least squares (MCR-ALS) method is a well-known multivariate self-modeling curve resolution procedure [43]. It facilitates a bilinear decomposition of the experimental data matrix according to the following algebraic model:

$$D = CS^T + E \quad (5)$$

where $\boldsymbol{D}$ is the experimental data matrix with dimensions, M (spectral objects) × N (wavelengths); $\boldsymbol{C}$ ($M \times F$) is the concentration profile matrix of F analytes in the samples; $\boldsymbol{S}^T$ ($F \times N$) is the transposed matrix consisting of, for example, the emission spectra; the F rows of this matrix contain the pure spectra associated with the F species in the samples; $\boldsymbol{E}$ ($M \times N$) is the residuals matrix. The number of F values is estimated by rank analysis, with the use of singular value decomposition (SVD), principal component analysis (PCA), or some related technique based on factor analysis, such as evolving factor analysis (EFA) [44]. The MCR-ALS procedure calculates the $\boldsymbol{C}$ and $\boldsymbol{S}$ matrices in turn by least squares, and the iterative process is repeated until convergence. When the number of species, F, and initial estimates, which are required to initiate the iterative ALS procedure [45], have been extracted, the concentration profile and pure spectra of all the contributing species can be established by the MCR-ALS method.

Parallel factor analysis (PARAFAC) is one of the commonly used algorithms for trilinear data decomposition, which can overcome the rotational freedom problem present with bilinear algorithms [46]. A PARAFAC model of a three-way array is given by three

loadings matrices, ***A***, ***B***, and ***C***, with elements a_{if}, b_{if} and c_{kf}, respectively. In the case of fluorescence excitation-emission data (EEM), PARAFAC decomposes the fluorescence signals, ***X***, into F tri-linear components according to the number of fluorophores present in the samples [47], and is expressed as Eq. (6):

$$x_{ijk} = \sum_{f=1}^{F} a_{if} b_{jf} c_{kf} + e_{ijk} \quad (6)$$

where x_{ijk} is the intensity of the measured light for sample, i, at excitation wavelength, j, and emission wavelength, k, and e_{ijk} is the error term; F is the number of factors. The ith score for the fth component is denoted by a_{if} and is related to the concentration of fluorophore, f, in the sample, i. Finally, b_{if} and c_{kf} are jth and kth elements of the fth emission and excitation loadings, respectively [48].

PARAFAC decomposition provides profile estimates for the three-way data. This indicates that the rank of the PARAFAC model is the same as the number of fluorescent compounds, f, which can be assigned to the analyte compounds; the loadings (a_{fi}, b_{fj} and c_{fk}) are the estimates of the relative concentrations of the analytes, emission spectra and excitation spectra for each of these compounds. Thus, the pure elementary spectra will be obtained if the correct number of factors (fluorophores) is used. The core consistency diagnostic indicates how well the model reflects the distribution of super-diagonal and off-super-diagonal elements of the Tucker3 core. If the PARAFAC model is correct, then it is expected that the super-diagonal elements will be close to one and the off-diagonal elements close to zero [49].

In this study, the number of factors for modeling was chosen by visual inspection of the excitation and emission profiles as well as by comparing the root mean square errors of calibration for successive models. In addition, the number of factors, i.e. constituents present in the samples, was also considered [50].

3. Results and discussion

3.1. Loading interaction of HCPT on GO

The HCPT UV–vis spectrum (green, Fig. 1A) shows several weak, broad bands in the 200–400 nm range, while the GO spectrum (blue) has one significant band of medium intensity at 230 nm (Section 2.3.1). The UV–vis spectrum from the HCPT–GO solution (red, Fig. 1A) is consistent with the spectrum (light blue, top, Fig. 1A) obtained by superimposing the absorption curve of HCPT on that of GO, i.e. the UV–vis spectrum of HCPT–GO complexes containing the HCPT peaks, is consistent with the absorption curve of GO when the two profiles are superimposed. This result reflects the interaction of HCPT and GO via a non-covalent interaction. This is consistent with previous work, that GO can form HCPT–GO complexes by a non-covalent, π–π stacking mechanism [51], and, their formation is assisted by hydrophobic interactions due to the aromatic nature of the HCPT molecule as well as its low solubility under basic conditions. The formation of this type of complex was further supported by a fluorescence study in this work, in which GO was added to HCPT. Free, unbound HCPT exhibited high fluorescence with two fluorescence peaks at 437 nm and 520 nm, but this fluorescence was quenched by the addition of GO at different concentrations (Fig. 1B). This quenching effect of HCPT by GO is consistent with the formation of the HCPT–GO complex, which, as previously noted, involves the π–π stacking interaction [51,52]. To follow this loading interaction quantitatively, the fluorescence spectral data matrix consisting of 25 fluorescence spectral objects and 501 wavelength variables was resolved by the MCR-ALS chemometrics method. The number of F chemical species involved in the interaction was estimated by EFA. Three significant factors were extracted, and this is

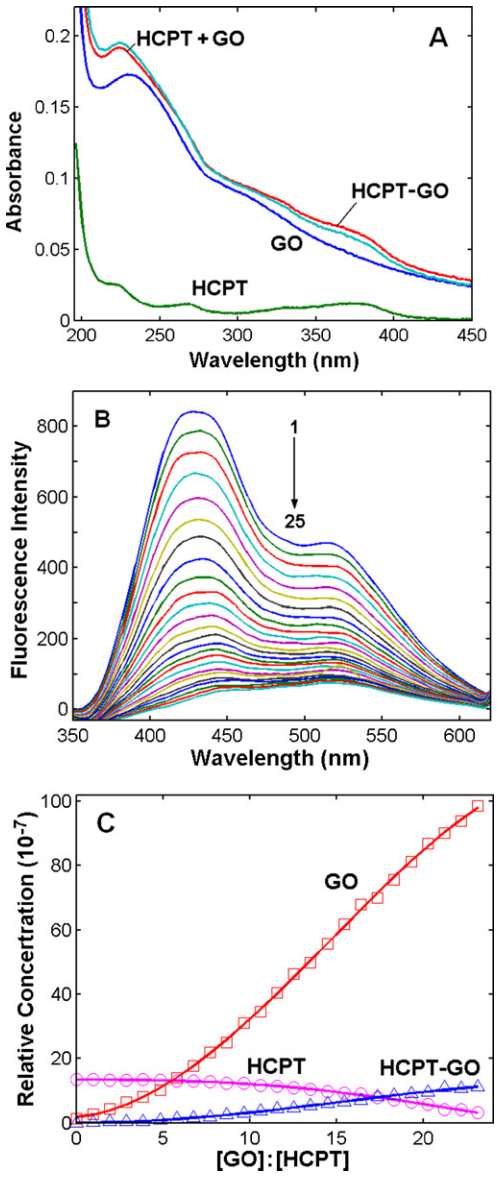

Fig. 1. (A) UV–vis absorbance spectra of HCPT (green),GO (blue), HCPT–GO complex (red) and HCPT + GO (light blue); (B) fluorescence emission spectra of HCPT (0.83 μg mL^{-1}) in Tris–HCl buffer solution after addition of GO (0.00–19.2 μg mL^{-1}); (C) recovered concentration profiles of HCPT, GO and BSA from the fluorescence data matrices with the use of MCR-ALS. (For interpretation of the references to color in this figure legend, the reader is referred to the web version of this article.)

consistent with the presence of HCPT, GO and the HCPT–GO complex; the concentration profiles obtained from the EFA processing, were used as the initial estimates for the three species in the MCR-ALS modeling. The relative concentration of HCPT decreased (mauve circles, Fig. 1C), while that of the HCPT–GO rose by about the same amount (blue triangles, Fig. 1C); the relative concentration of GO rose sharply (red squares, Fig. 1C) and this indicated an excess of unreacted GO sites. These observations are consistent with the formation of an HCPT–GO complex presumably formed by the HCPT π–π stacking on the GO surface.

3.2. Binding interaction between HCPT and BSA

BSA fluoresces naturally at 350 nm after excitation at 280 nm, and this fluorescence is related to the tryptophan residues [53]. Binding of small molecules with BSA can quench this effect, as illustrated by the decreasing fluorescence spectra of BSA obtained

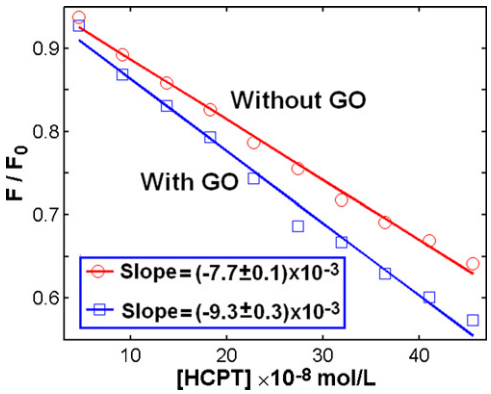

Fig. 2. Relative fluorescence changes (F/F_0) of BSA (1.0×10^{-7} mol L^{-1}) at different concentrations of HCPT ($0.00–4.56 \times 10^{-7}$ mol L^{-1}) with and without GO (2.96 μg mL^{-1}) in a Tris–HCl buffer solution. F_0 and F are the fluorescence intensity without and with HCPT, respectively.

by the addition of increasing amounts of the HCPT ligand (see Supplementary material, Fig. S-1A). The BSA fluorescence intensity decreased and new fluorescence peaks developed at longer wavelengths as a function of increasing HCPT concentration. An isoactinic point formed at 403 nm, which indicated an equilibrium between the free HCPT and the formed HCPT–BSA complex. In addition, with the addition of HCPT, the major fluorescence peak showed a slight shift revealing that the microenvironment around the tryptophan residues was progressively affected by the interaction with HCPT.

The Stern–Volmer quenching constants, K_{SV}, obtained at each of the two temperatures (Section 2.3.2), were inversely correlated with temperature, which indicated that the binding interaction was initiated by static quenching. The quenching appeared to be more effective in the presence of GO (Supplementary material, Fig. S-1B) suggesting that GO somewhat promoted the binding interaction of HCPT with the BSA as indicated by the slightly different slopes ($(-9.3 \pm 0.3) \times 10^{-3}$ and $(-7.7 \pm 0.1) \times 10^{-3}$, respectively; Fig. 2).

The binding constants, K_a, and thermodynamic parameters ($\Delta H = -22.3$ kJ mol^{-1}, $\Delta G = -35.0$ kJ mol^{-1}, and $\Delta S = 42.6$ J mol^{-1} K^{-1}) involved in the binding interaction were obtained from the fluorescence data. According to the theory proposed by Ross and Subramanian [54], the negative ΔH and positive ΔS values for the binding reaction suggested that HCPT was bound to the BSA mainly by hydrophobic interactions and electrostatic forces. As well, the presence of GO strengthened this binding as indicated by the increase in the K_a from $(1.38 \pm 0.01) \times 10^6$ to $(1.61 \pm 0.03) \times 10^6$ L mol^{-1}.

To explore the binding interaction further, two three-way excitation-emission fluorescence spectral matrices of the HCPT–BSA system, with and without GO, were collected, and a three component PARAFAC model was developed to resolve these two arrays; these included the data from the overlapping spectral profiles. Thus, the concentration profiles of the two reactant analytes, HCPT and BSA, could be extracted. These profiles of the two analytes (Fig. 3A) showed that: 1. in the HCPT–BSA system, the free BSA concentration was almost unchanged with the addition of HCPT, and the concentration of HCPT increased almost at the same rate as that of the addition of HCPT; this suggested that the binding interaction between HCPT and BSA was weak; 2. when GO was present in the system, the concentration of BSA clearly decreased, and that of HCPT moderately increased in comparison with the concentrations in the previous case; this suggested that GO promoted the binding of HCPT to BSA, and thus, GO apparently can facilitate the delivery of HCPT to BSA.

The excitation and emission loadings values extracted by the PARAFAC method for BSA and HCPT compared well with the

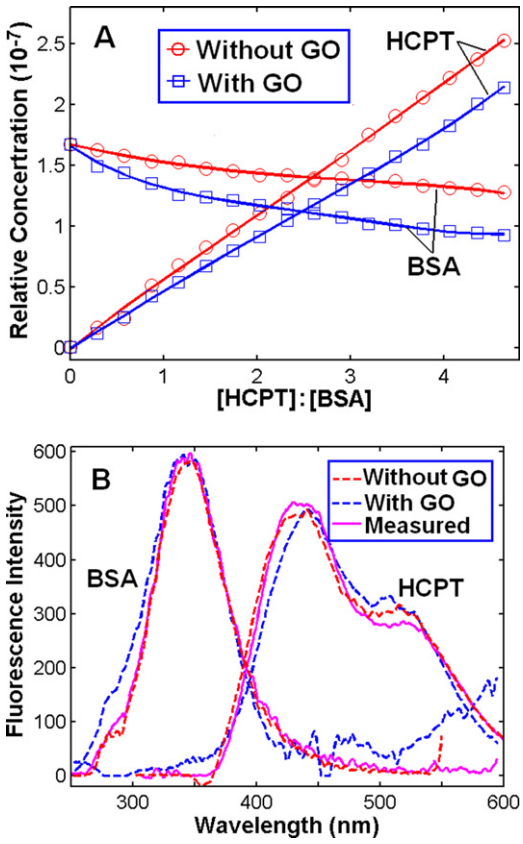

Fig. 3. (A) Relative concentrations for BSA and HCPT extracted by PARAFAC; (B) estimated emission spectra of BSA (dashed lines) and HCPT in the reaction mixture compared to the measured ones (solid line).

measured ones (Fig. 3B). This supported the results extracted by the PARAFAC method.

3.3. BSA induced fluorescence enhancement of HCPT loaded on GO

The fluorescence quenching of HCPT based on fluorescence resonance energy transfer (FRET) between HCPT and GO was investigated with the use of fluorescence spectra. Interestingly, a red shift of the fluorescence emission peak was noted and its intensity increased considerably when BSA was added to the HCPT–GO complex solution (Fig. 4). A control experiment showed that when HCPT was added to BSA in the absence of GO, only a weak response was observed (Supplementary material, Fig. S-2). This indicated that GO was necessary to achieve the enhanced fluorescence response. To further understand the processes involved in the fluorescence enhancement attributed to the presence of BSA, the interaction between BSA and GO was investigated by the fluorescence quenching method. The fluorescence intensity of BSA decreased with increasing concentrations of GO (Fig. 5). GO has a high non-specific affinity for bio-macromolecules such as proteins and DNA, and the adsorption of BSA on the surface of GO has been reported in a study for the preparation of BSA–GO conjugates [55]. In that work, the BSA adsorbed on GO ensured that this protein was close to HCPT, and this facilitated the energy transfer. Since graphene is a good energy acceptor and has a large specific surface area, it is reasonable to suggest that the fluorescence enhancement of the HCPT–GO complex in solution induced by BSA, was the result of the formation of the HCPT–BSA complex on the surface of GO. Thus, when added, BSA was absorbed on the surface of GO, and also, it combined with the HCPT on GO; the formation of the BSA–GO complex

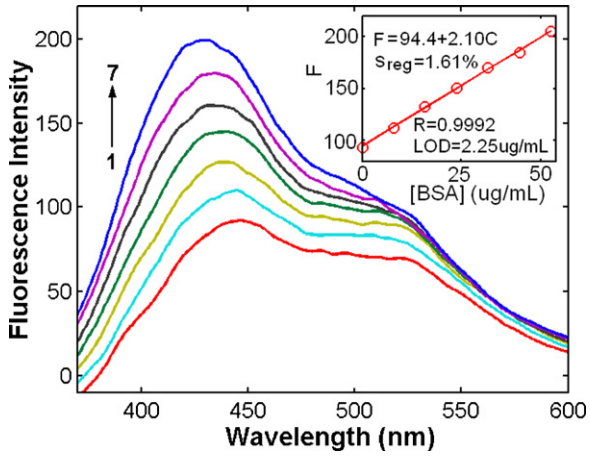

Fig. 4. Fluorescence spectra of HCPT–GO in the presence of BSA at different concentrations (0.00–7.98 × 10^{-7} mol L^{-1}) in a Tris–HCl buffer solution. Insert: fluorescence intensity versus concentration of BSA. Excitation wavelength: 320 nm.

prevented the HCPT from interacting with the GO surface. Thus, the fluorescence of HCPT recovered. Also, the emission peak of BSA blue-shifted (~10 nm) with the addition of GO, which indicated that the microenvironment around the tryptophan residues was affected by GO; it probably provided a more rigid and hydrophobic environment. These favorable hydrophobic characteristics could facilitate the transfer of HCPT to BSA and its subsequent complex formation with this protein. The binding site of BSA prevented the free rotor motions in the HCPT molecule moiety; this phenomenon may have enhanced the fluorescence and the spectral blue shift of HCPT [56]. Clearly, the system benefited from using GO (Scheme 1), whose complex formation with HCPT decreased the fluorescence, and the addition of BSA facilitated the fluorescence enhancement.

3.4. Ternary system of HCPT, BSA, and GO

The above investigation demonstrated that both HCPT and BSA can complex with GO via non-covalent interactions. GO apparently promoted the interaction between HCPT and BSA, and BSA probably induced fluorescence turn-on of the HCPT–GO complex solution. To obtain further evidence for these observations, the HCPT/GO/BSA reaction system was studied with the use of the resonance light scattering (RLS) technique.

In general, when molecules aggregate, they produce enhanced light scattering effects, which commonly produce bands that are many times more intense than any molecular absorption bands; such strong RLS bands occur in the vicinity of the original

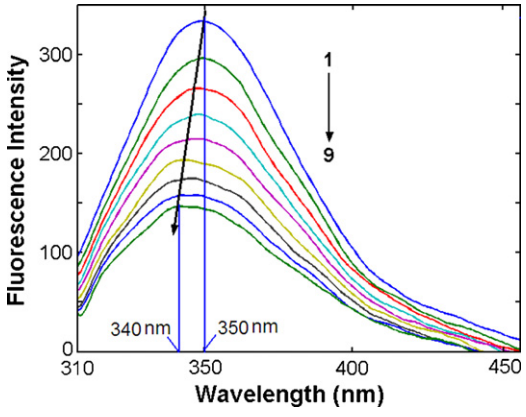

Fig. 5. Fluorescence quenching of BSA spectra (1.0 × 10^{-7} mol L^{-1}) on addition of GO (0.00–2.7 μg mL^{-1}) in Tris–HCl buffer solution.

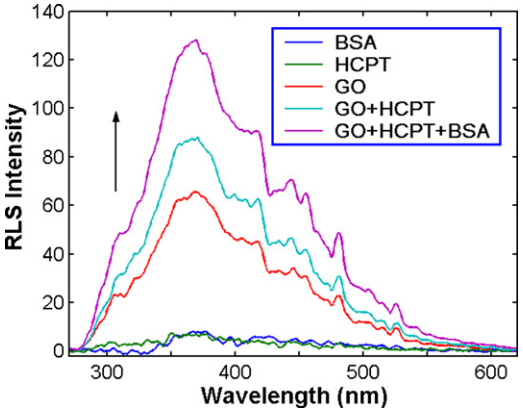

Fig. 6. Resonance light scattering spectra of the HCPT–BSA–GO system, [BSA] = 1.0 × 10^{-7} mol L^{-1}, [HCPT] = 4.57 × 10^{-7} mol L^{-1}, and [GO] = 2.96 μg mL^{-1}.

absorption band [57]. Thus, as the molecular stack grows so does the intensity of the RLS band. This is exactly what was observed (Fig. 6) – both free HCPT and BSA exhibited low RLS signals, and the RLS response of free GO was comparatively favorable. The RLS intensity of GO was enhanced when HCPT and BSA were added into the GO solution, especially since the intensity reached a peak in the presence of both HCPT and BSA. The RLS spectra were closely correlated to some intrinsic behaviors of the complex and suggested that a HCPT–BSA–GO ternary complex may be formed in the system. Therefore, these results strongly supported the HCPT–GO–BSA complex formed in the system as proposed on the basis of the UV–vis and fluorescence spectroscopy above.

The various molecular species, GO, HCPT–GO, BSA–GO and HCPT–BSA–GO, should have different surface morphologies and sizes; this aspect was investigated with the use of atomic force microscopy (AFM) in the tapping mode (Fig. 7). The thickness of GO was estimated to be about 0.93 nm (Fig. 7A), which is in good agreement with the literature [58]. On addition of HCPT, the height of the image layer was increased to about 1.32 nm (Fig. 7A), and the surface appeared rather granulated in comparison with that of GO alone (Fig. 7B); this could indicate that the medicinal drug molecules were partially absorbed into the GO layer causing a slight swelling and hence, an increase in height. Also, when BSA was added to GO, the aggregate height increased to 3.09 nm as a result of the large protein molecule binding non-covalently on the GO surface. Finally, after the addition of both HCPT and BSA to GO, the height of the image layer increased to 3.74 nm; this is a further indication that both HCPT and BSA aggregated on the surface of GO. In addition, as the height of the deposit increased so did its roughness; this observation is in agreement with the formation of roughly uniform HCPT/BSA aggregates on the surface of GO. The interaction mechanism between HCPT, BSA, and GO is presented in Scheme 1. HCPT can be bound to GO to form an HCPT–GO complex through noncovalent interactions. The added BSA may be partially adsorbed on the GO surface, and bind with HCPT on GO through hydrophobic interactions with higher affinity. This may explain HCPT's improved delivery to the protein in the presence of GO.

3.5. BSA detection based on fluorescence enhancement

The fluorescent biosensing platform based on GO could result in a fluorescence-enhanced detection, which is sensitive to BSA. The potential of this suggestion was experimentally tested by measuring the fluorescence output from a series of BSA samples at different concentrations in the presence of the HCPT–GO biosensor. The intensity increased sequentially in proportion to the BSA concentration (Fig. 4 and insert). The linear plot (regression coefficient,

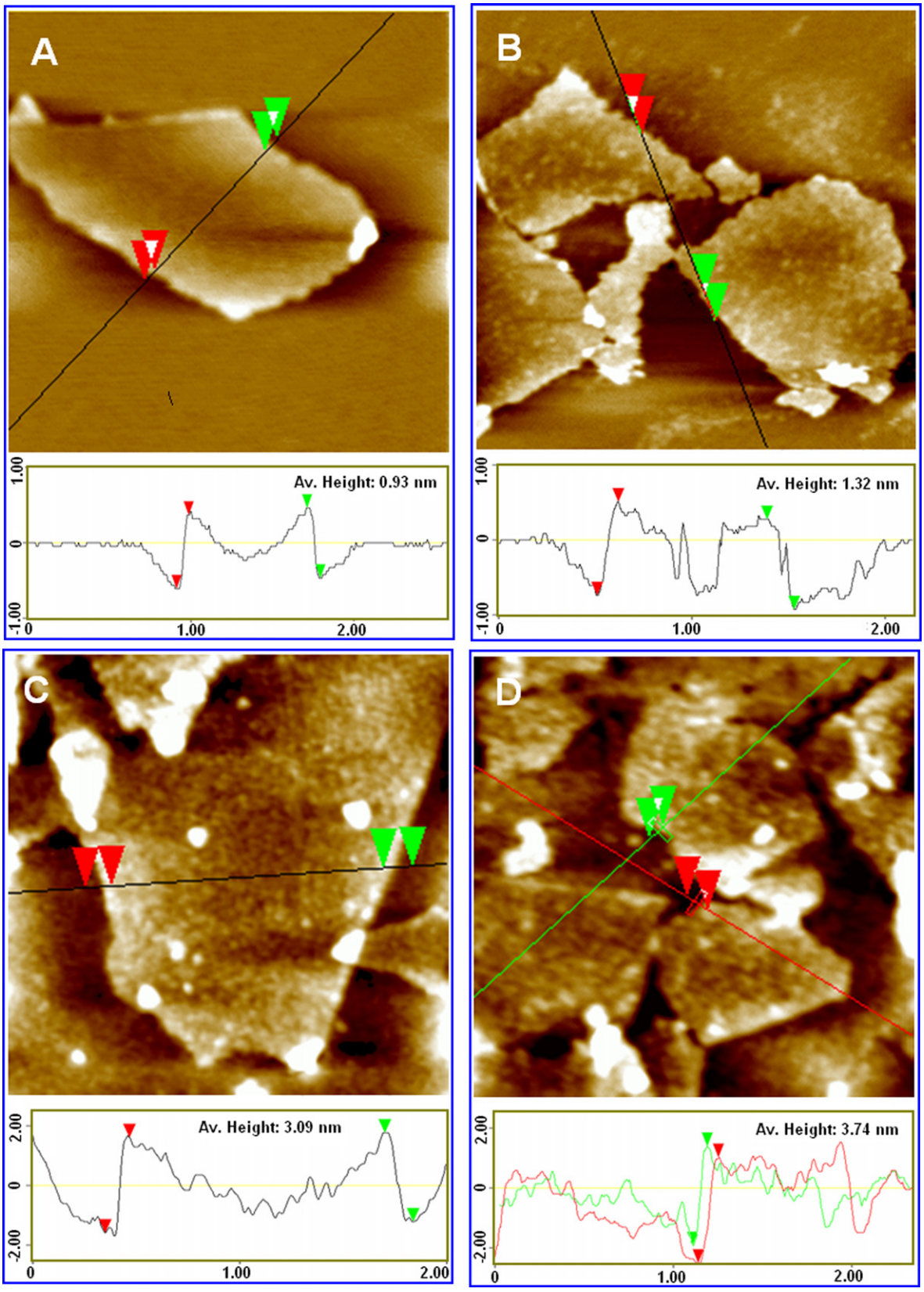

Fig. 7. AFM images of: (A) GO, (B) HCPT–GO, (C) BSA–GO, and (D) HCPT–BSA–GO. Scan size is 2.0 μm × 2.0 μm, [GO] = 25 μg mL^{-1}.

R = 0.9992; regression standard deviation, s_{reg} = 1.61%) over the BSA concentration range of 0.00–52.67 μg mL^{-1} indicated a detection limit of 2.25 μg mL^{-1}; this value was much better than those reported for the other aggregation-induced emission biosensors (limit of detection: 26.4 μg mL^{-1}) [59]. Also, in three parallel experiments involving a sample with BSA, the enhancement of relative fluorescence intensity had a satisfactory reproducibility as reflected by the standard deviation of ±3.1%. The kinetics of HCPT and GO

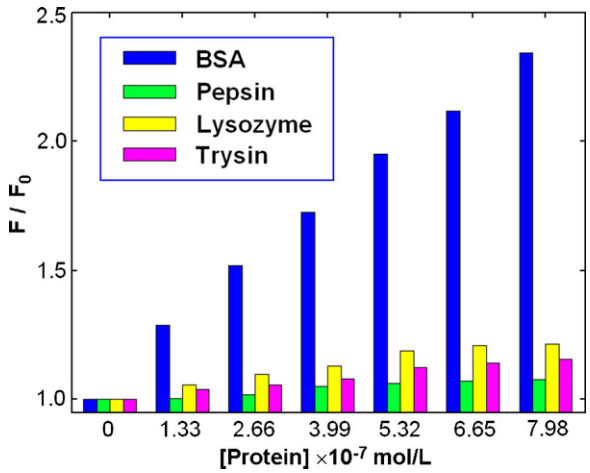

Fig. 8. Relative fluorescence changes of HCPT–GO as function of BSA, lysozyme, pepsin, and trypsin at different concentrations (relative fluorescence ratio (F/F_0) – definition see Fig. 2).

interaction, as well as that of the HCPT–GO complex with BSA, were studied by monitoring the fluorescence intensity as a function of time. Both the adsorption of HCPT on the surface of GO and the competitive binding of BSA with GO for HCPT were very fast at room temperature; all interactive components reached equilibrium within 2 min. Thus, the GO-based fluorescence approach can detect BSA in real time, consequently, improving its applicability. On the other hand the detection range was found to be relatively narrow. The underlying explanation for this may lay in the observation that the main reason for fluorescence enhancement may be due to the fluorescence of HCPT being quenched by GO but also be enhanced on addition of BSA (see Section 3.3). Thus, the net fluorescence is derived from a more complex process in which the loading ratio of HCPT to GO may play an important role. However, the investigation of this suggestion is beyond the scope of the present work.

In order to investigate the selectivity of the GO based biosensor, control experiments were carried out with the use of another three proteins, lysozyme, pepsin, and trypsin, instead of BSA, under the same conditions. The relative fluorescence (F/F_0) values were quite low in the cases of the lysozyme and pepsin proteins (Fig. 8). In contrast, the relative fluorescence values for BSA were comparatively high and the plot was linear as a function of the BSA analyte concentration. This indicated that the HCPT–GO biosensor was selective for the BSA protein. This result may be attributed to the hydrophobic interaction between HCPT and BSA [60].

4. Conclusions

Investigation of the HCPT/GO/BSA interaction with the aid of UV–vis and fluorescence spectroscopic methods revealed that HCPT can be adsorbed on the surface of GO by simple mixing of the two substances to form an HCPT–GO complex. However, fluorescence emission intensity is significantly enhanced with the addition of the BSA; this protein also facilitates the formation of the HCPT–GO–BSA complex and the quantitative analysis for BSA. This novel method is sensitive and quite selective for BSA. On the other hand the detection range was found to be relatively narrow, and the net fluorescence may be derived from a more complex process in which the loading ratio of HCPT to GO may play an important role.

The above results also suggest that the method facilitates the use of GO to load and deliver HCPT to proteins, i.e. this opens up the potential use of these substances for medicinal drug delivery. Thus, a bio-sensing platform was developed for fluorescence-enhanced detection based on GO, and the satisfactory performance and low costs of the GO-based fluorescence-enhanced biosensors suggests a promising future in clinical diagnostics and treatment.

Acknowledgements

The authors gratefully acknowledge the financial support of this study by the National Natural Science Foundation of China (NSFC-21065007), the Jiangxi Provincial Education Department Science Foundation (GJJ10037), the Graduate Student Innovation Program of Nanchang University (YC2012-S012), and the State Key Laboratory of Food Science and Technology of Nanchang University (SKLF-MB-201002 and SKLF-TS-200919).

Appendix A. Supplementary data

Supplementary data associated with this article can be found, in the online version, at http://dx.doi.org/10.1016/j.aca.2013.01.038.

References

[1] K.N. Burger, R.W. Staffhorst, H.C. de Vijlder, P.H. Bomans, P.M. Frederik, B. de Kruijff, Nat. Med. 8 (2002) 81.
[2] W. Wei, G.H. Ma, G. Hu, D. Yu, T. Mcleish, Z.G. Su, Z.Y. Shen, J. Am. Chem. Soc. 130 (2008) 15808.
[3] L.Y. Tang, Y.C. Wang, Y. Li, J.Z. Du, J. Wang, Bioconjugate Chem. 20 (2009) 1095.
[4] S. Santra, C. Kaittanis, J. Grimm, J.M. Perez, Small 5 (2009) 1862.
[5] R. Guo, R.T. Li, X.L. Li, L. Zhang, X.Q. Jiang, B. Liu, Small 5 (2009) 709.
[6] S. Purushotham, R.V. Ramanujan, Acta Biomater. 6 (2009) 502.
[7] K.S. Novoselov, A.K. Geim, S.V. Morozov, D. Jiang, Y. Zhang, S.V. Dubonos, I.V. Grigorieva, A.A. Firsov, Science 306 (2004) 666.
[8] D.A. Dikin, S. Stankovich, E.J. Zimney, R.D. Piner, G.H.B. Dommett, G. Evmenenko, S.T. Nguyen, R.S. Ruoff, Nature 448 (2007) 457.
[9] A.K. Geim, K.S. Novoselov, Nat. Mater. 6 (2007) 183.
[10] J. Wu, W. Pisula, K. Mllen, Chem. Rev. 107 (2007) 718.
[11] G. Eda, G. Fanchini, M. Chhowalla, Nat. Nanotechnol. 3 (2008) 270.
[12] Y. Kopelevich, P. Esquinazi, Adv. Mater. 19 (2007) 4559.
[13] X.L. Li, X.R. Wang, L. Zhang, S.W. Lee, H.J. Dai, Science 319 (2008) 1229.
[14] J. Zhan, G.F. Chen, L. Zhu, G.X. Li, Electrochem. Commun. 13 (2011) 31.
[15] S. Stankovich, D.A. Dikin, G.H.B. Dommett, K.M. Kohlhaas, E.J. Zimney, E.A. Stach, R.D. Piner, S.T. Nguyen, Nature 442 (2006) 282.
[16] D. Li, M.B. Müller, S. Gilge, R.B. Kaner, G.G. Wallace, Nat. Nanotechnol. 3 (2008) 101.
[17] X.M. Sun, Z. Liu, K. Welsher, J.T. Robinson, A. Goodwin, S. Zaric, H.J. Dai, Nano Res. 1 (2008) 203.
[18] Z. Liu, J.T. Robinson, X.M. Sun, H.J. Dai, J. Am. Chem. Soc. 130 (2008) 10876.
[19] X.Y. Yang, X.Y. Zhang, Z.F. Liu, Y.F. Ma, Y. Huang, Y.S. Chen, J. Phys. Chem. C 112 (2008) 17554.
[20] L.M. Zhang, J.G. Xia, Q.H. Zhao, L.W. Liu, Z.J. Zhang, Small 6 (2010) 537.
[21] J. Balapanuru, J.X. Yang, S. Xiao, Q.L. Bao, M. Jahan, L. Polavarapu, J. Wei, Q.H. Xu, K.P. Loh, Angew. Chem. Int. Ed. 122 (2010) 6699.
[22] H.F. Dong, W.C. Gao, F. Yan, H.X. Ji, H.X. Ju, Anal. Chem. 82 (2010) 5511.
[23] Y.Q. Xu, M.M. Guo, X.P. Li, A. Malkovskiy, C. Wesdemiotis, Y. Pang, Chem. Commun. 47 (2011) 8883.
[24] S. Myung, A. Solanki, C. Kim, J. Park, K.S. Kim, K. Lee, Adv. Mater. 23 (2011) 2221.
[25] Y.Q. Wen, F.F. Xing, S.J. He, S.P. Song, L.H. Wang, Y.T. Long, D. Li, C.H. Fan, Chem. Commun. 46 (2010) 2596.
[26] Y.X. Xu, L. Zhao, H. Bai, W.J. Hong, C. Li, G.Q. Shi, J. Am. Chem. Soc. 131 (2009) 13490.
[27] T. Zhang, Z.G. Cheng, Y.B. Wang, Z.J. Li, C.X. Wang, Y.B. Li, Y. Fang, Nano. Lett. 10 (2010) 4738.
[28] Y. Wang, Z.H. Li, D.H. Hu, C.T. Lin, J.H. Li, Y.H. Lin, J. Am. Chem. Soc. 132 (2010) 9274.
[29] Y. Shi, W.T. Huang, H.Q. Luo, N.B. Li, Chem. Commun. 47 (2011) 4676.
[30] Y.L. Leu, C.S. Chen, Y.J. Wu, J.W. Chern, J. Med. Chem. 51 (2008) 1740.
[31] H. Malonga, J.F. Neault, H.A. Tajmir-Riahi, DNA Cell Biol. 25 (2006) 393.
[32] C. Mancuso, A. Bonsignore, C. Capone, Antioxid. Redox Signal 8 (2006) 3.
[33] C.H. Lu, H.H. Yang, C.L. Zhu, X. Chen, G.N. Chen, Angew. Chem. Int. Ed. 48 (2009) 4785.
[34] H.X. Chang, L.H. Tang, Y. Wang, J.H. Jiang, J.H. Li, Anal. Chem. 82 (2010) 2341.
[35] C. Bertucci, S. Cimitan, A. Riva, P. Morazzoni, J. Pharm. Biomed. Anal. 42 (2006) 81–87.
[36] Z. Liu, X.M. Sun, N. Nakayama-Ratchford, H.J. Dai, ACS Nano 1 (2007) 50.
[37] Y.Q. Wang, H.M. Zhang, G.C. Zhang, W.H. Tao, S.H. Tang, J. Lumin. 126 (2007) 211.
[38] Y.N. Ni, S. Du, S. Kokot, Analyst 134 (2009) 1840.
[39] J.R. Lakowicz, Principles of Fluorescence Spectroscopy, 3rd ed., Springer Press, New York, 2006.
[40] J.B. Yu, B. Li, P. Dai, S.G. Ge, Spectrochim. Acta A 74 (2009) 277.

[41] D. Leckband, Annu. Rev. Biophys. Biomol. Struct. 29 (2000) 1.
[42] X.R. Wang, X.Y. Xie, C.L. Ren, Y. Yang, X.M. Xu, X.G. Chen, Food Chem. 127 (2011) 705.
[43] R. Tauler, Chemom. Intell. Lab. Syst. 30 (1995) 133.
[44] H. Gampp, M. Maeder, C.J. Meyer, A.D. Zuberbuhler, Talanta 33 (1986) 943.
[45] M. Vives, R. Gragallo, R. Tauler, Anal. Chim. Acta 424 (2000) 105.
[46] Y.N. Li, H.L. Wu, J.F. Nie, S.F. Li, Y.J. Yu, S.R. Zhang, R.Q. Yu, Anal. Methods 1 (2009) 115.
[47] D.B. Gil, A.M. de la Pena, J.A. Arancibia, G.M. Escandar, A.C. Olivieri, Anal. Chem. 78 (2006) 8051.
[48] R. Bro, Chemom. Intell. Lab. Syst. 38 (1997) 149.
[49] S. Engelen, S. Frosch, B.M. Jorgensen, J. Chemom. 23 (2009) 124.
[50] M.G. Trevisan, R.J. Poppi, Anal. Chim. Acta 493 (2003) 69.
[51] R.J. Chen, Y.G. Zhang, D.W. Wang, H.J. Dai, J. Am. Chem. Soc. 123 (2001) 3838.
[52] N. Nakayama-Ratchford, S. Bangsaruntip, X.M. Sun, K. Welsher, H.J. Dai, J. Am. Chem. Soc. 129 (2007) 2448.
[53] B.F. Pan, F. Gao, L.M. Ao, J. Magn. Magn. Mater. 293 (2005) 252.
[54] P.D. Ross, S. Subramanian, Biochemistry 20 (1981) 3096.
[55] J.B. Liu, S.H. Fu, Y.L. Li, Z.X. Deng, J. Am. Chem. Soc. 132 (2010) 7279.
[56] H. Tong, Y.N. Hong, Y.Q. Dong, M. Häussler, Z. Li, J.W.Y. Lam, Y.P. Dong, H.H.-Y. Sung, I.D. Williams, B.Z. Tang, J. Phys. Chem. B 111 (2007) 11817.
[57] J.B. Xiao, J. Shi, H. Cao, S.D. Wu, F.L. Ren, M. Xu, J. Pharm. Biomed. Anal. 45 (2007) 609.
[58] Y.X. Xu, H. Bai, G.W. Lu, C. Li, G.Q. Shi, J. Am. Chem. Soc. 130 (2008) 5856.
[59] X.J. Xu, J. Huang, J.J. Li, J.W. Yan, J.G. Qin, Z. Li, Chem. Commun. 47 (2011) 12385.
[60] Y.Q. Xu, A. Malkovskiy, Y. Pang, Chem. Commun. 47 (2011) 6662.